International Journal of Mass Spectrometry 280 (2009) 119–127

Contents lists available at ScienceDirect

International Journal of Mass Spectrometry

journal homepage: www.elsevier.com/locate/ijms

State-specific reactions and autoionization dynamics of Ar^{2+} produced by synchrotron radiation

Pietro Franceschi[a], Roland Thissen[b,*], Odile Dutuit[b], Christian Alcaraz[c], Heloise Soldi-Lose[c], Davide Bassi[a], Daniela Ascenzi[a], Paolo Tosi[a], Jan Zabka[d], Zdenek Herman[d], Marcello Coreno[e], Monica de Simone[f]

[a] *Dipartimento di Fisica, Università di Trento, Via Sommarive 14, Povo, Trento, Italy*
[b] *Laboratoire de Planétologie de Grenoble, CNRS UMR 5109, UJF Bâtiment D de physique, 120 rue de la piscine, 38041 Grenoble, France*
[c] *Laboratoire de Chimie Physique, CNRS UMR 8000, Université Paris-Sud, Orsay, France*
[d] *V. Čermàk Laboratory, J. Heyrovsky Institute of Physical Chemistry, Acad. Sci. of the Czech Republic, Dolejškova 3, 182 23 Praha 8, Czech Republic*
[e] *CNR – IMIP, Rome Branch c/o Gasphase Beamline@Elettra, Trieste, Italy*
[f] *CNR – Laboratorio Nazionale TASC, INFM, Trieste, Italy*

ARTICLE INFO

Article history:
Received 2 June 2008
Received in revised form 11 July 2008
Accepted 18 July 2008
Available online 30 July 2008

Keywords:
Argon
Dication
Photoionization
Ion molecule reaction
Autoionization

ABSTRACT

The long-lived excited states of doubly charged rare gases can markedly affect their reactivity. In this paper we demonstrate the presence of strong state-specific effects in the charge exchange of Ar^{2+} (^3P, ^1D and ^1S) with several neutral targets (He, Ne, Kr, Xe, D_2, and CH_4). State sensitive measurements have been performed by producing the different Ar^{2+} electronic states via tunable synchrotron radiation (Elettra-Trieste, Italy and SuperACO-Orsay, France). From the product ion yield data of charge transfer, state-selected total cross-sections have been deduced. Using the state-specific reactivity of Ar^{2+} towards different neutral targets, it has been possible to extract the photon-energy-dependent production branching of the three doubly charged states and to investigate the autoionization dynamics of neutral or singly charged Ar in the vicinity of the double ionization threshold.

1. Introduction

The reactions of doubly charged ions are important in many ionized media including plasmas, ionospheres and astrophysical environments, where charged species are produced by high energy electrons and photons. In the case of rare gas atoms, ionization can produce excited states whose radiative quenching to the ground state is forbidden. Such long-lived species hold a large amount of internal energy which may influence their reactivity.

One-photon double ionization is forbidden in the frozen orbital-independent particle model; however it widely occurs due to electron correlations. For Ar dication, three different ionic states (^3P, ^1D and ^1S) can be populated in the 43–52 eV energy range. The threshold of the ^3P ground state occurs at 43.39 eV, the onset of the ^1D lies at 45.13 eV, while, at even higher energies, the ^1S opens up at 47.51 eV [1].

The branching ratios of the three states have been reported in a two electron coincidence measurement [2] performed at 48.4 eV photon energy. It led to the conclusion that the three dicationic states are populated according to their statistical weights. This near statistical population of dication final states was quite unexpected for two reasons: (i) according to the Wannier law, the partial cross-section for double ionization rises approximately linearly from threshold amplifying the final states of lowest energy and (ii) extended Wannier theory [3] states that, for symmetry reasons, the ^3P final state is the most favored one in direct double ionization near threshold. Spectra of Eland et al. [2] contain intense features associated to autoionization of singly charged ions and are responsible for the near statistical population of the final states. Eland et al. comes to the conclusion that "our understanding of the processes of double photoionization and of autoionization branching is still unsatisfactory". In the present work, we profit from target-dependent state-specific reactivity and photon energy-dependent measurements to deduce the branching ratio of the three states from double ionization threshold up to 52 eV.

Charge transfer, quenching and association reactions of doubly charged rare gas ions were thoroughly investigated in drift tube-mass spectrometer (SWARM) experiments by Johnsen and Biondi

* Corresponding author.
E-mail address: Roland.Thissen@obs.ujf-grenoble.fr (R. Thissen).

1387-3806/$ – see front matter © 2008 Elsevier B.V. All rights reserved.
doi:10.1016/j.ijms.2008.07.020

[4,5]. State-selected rate constants for the reactions of Ar^{2+} (and all the other rare gas dications) with rare gases were measured. State selection was obtained by profiting from the different mobilities of various ionic states in the buffer gas [6]. In addition, to obtain "pure" ionic beams, the authors took advantage of the quenching of selected Ar^{2+} states when Ar or He were used as buffer gases. Under these conditions, the rate constant for ^1D reactivity was given only as a rough estimate, since the mobility signal of this state overlapped with the ^3P signal and since collisional quenching could have contributed to the loss of ^1D ions. In the same paper, experimental results were rationalized by the relative positions of the diabatic potential energy curves for the $X^{2+} + Y$ and $X^+ + Y^+$ systems. Reactions with exothermicities of ~4 eV turn out to be fast, in good agreement with the "reaction window" model based on the Landau Zener formalism [7,8] and the small reaction rate constant for excited state reactants is as expected with this energy-defect criterion.

Almost at the same time, another series of investigations was performed by means of drift experiments [9–12]. Neutral targets range from rare gas atoms (helium, argon and xenon) to molecules (H_2, N_2, O_2, CO_2, CH_4, C_2H_2, and NO_2). It is worth noting that, in these experiments, state-selection over the dication electronic states was obtained by using chemical reactions with a buffer gas in order to selectively remove some Ar^{2+} states from the mixture produced in the ion source, as indicated by Johnsen and Biondi [4].

At low temperatures (30 K), rate constants for some Ar^{2+} (^3P) reactions were investigated in CRESU experiments [13].

In the case of the Ar^{2+} + He reaction, state-selected information was obtained in a crossed beam experiment, where it was possible to distinguish the relative contributions of the Ar^{2+}(^3P, ^1D) states to the reactive cross-section [14]. The outcomes of this experiment were interpreted by quasi-classical calculations [15], deriving a rate constant of k (300 K) = 4.4×10^{-12} cm^3 s^{-1} for the charge transfer involving the ^3P state.

The results of all previous investigations will be discussed in Section 3 of the present paper. However, it is possible to point out some general observations concerning previous work: (i) in the majority of cases, state-selected information on the reactivity has been obtained only by using the state selective removal of Ar^{2+} by reaction with a buffer gas. The validity of this somehow "self-referential" approach has never been independently verified and (ii) for most of the neutral targets, no definitive results on Ar^{2+} (^1D) reactivity have been obtained.

In the last years, our research groups investigated the properties of doubly charged atomic and molecular systems: we studied dication thermodynamics [16,17], ion-molecule reactions involving dications [18–23], we measured internal energy effects in the reactivity of CO_2^{2+} [24] and, more recently, we investigated the dynamics of the double photoionization process producing N^{2+} from N_2 [25]. We also investigated the implications of our work for the modelling of planetary atmospheres [26,27].

The present paper reports on strong state-specific effects detected in the cross-section of charge transfer reactions between doubly charged ions Ar^{2+} and several neutral targets (He, Ne, Kr, Xe, D_2, and CH_4). In the experiment, the different Ar^{2+} states were populated by using tunable synchrotron radiation from two storage rings, Super-ACO (LURE-Paris) and ELETTRA (Sincrotrone Trieste, Trieste). State sensitivity was revealed by varying the photon energy from 43 to 52 eV and measuring the evolution of the absolute reaction cross-section. The study of multiple targets made it possible to investigate the details of the double ionization process of Ar atoms and to correlate specific reactivity with either the ground and/or the metastable states of the dication. No removal of ionic state is necessary in this case. Furthermore, assuming a statistical production of the three states, we estimate the state-selected cross-sections for the charge transfer processes and finally, using all the information, we extract an energy-dependent production branching ratio for the three dicationic states in the investigated energy range. This result is particularly interesting, since it allows identification of photon energy-dependent double ionization mechanisms towards the different final states. Such information at each photon energy would require time-consuming measurements of the two photoelectrons and of their kinetic energy in coincidence.

2. Experimental

Charge transfer cross-sections were measured using the CERISES [20,28] apparatus installed first at the undulator beamline SU6 of the Super-ACO storage ring (LURE-Paris) and, subsequently, on the branch line of the gas phase photoemission beamline at the ELETTRA synchrotron radiation facility (Trieste, Italy). The CERISES apparatus is a tandem mass spectrometer composed of two octopoles located between two quadrupole mass spectrometers in a *Q1-O1-O2-Q2* configuration (where *Q* stands for quadrupole and *O* for octopole) placed in three differentially pumped regions. Such a configuration permits investigation of both uni- and bi-molecular reactions of mass-selected ions. In the source region, Ar^{2+} ions were produced by double photoionization of Ar by synchrotron radiation. After ionization, ions were extracted from the source by a small field of 1 V/cm, and injected through a stack of electrodes into the quadrupole mass filter *Q1*. At the exit of this filter, ions were refocused into the *O1* radio frequency ion guide towards the reaction cell. Depending on the acceleration potential, the reactant ions produced in the source needed at most 40 μs to reach the reaction cell. Dication reactions took place in a 4-cm long scattering cell filled with the neutral target gas (He, Ne, Kr, Xe, D_2, and CH_4) at room temperature. The absolute value of their pressure was measured by a Baratron capacitance manometer and adjusted to a value ≈10^{-4} mbar to ensure single-collision conditions. The reactant ion kinetic energy is defined by the dc potential difference between the collision cell octopole and the center of the ion source. It can be varied between 0.4 and 40 eV in the laboratory energy frame, with a typical distribution width of 0.5 eV full width at half maximum (FWHM). Reactant and product ions were confined by the radio frequency guiding field of *O1*, guided by *O2*, mass selected in the *Q2* mass filter, and finally detected by a multichannel plate detector. Data were recorded according to a procedure described in Ref. [28]. The total electron yield resulting from Ar photoionization in the ion source was recorded during all measurements to correct for any variation of the Ar pressure. Photon energy scans, collecting ionic yields of Ar^{2+} and Ar^+ with and without the neutral target gas in the reaction cell permit to correct for any contribution to reactivity occurring outside the calibrated reaction cell [29]. Photoion signals were normalized to the incident photon flux as a function of photon energy. Effective absolute cross-sections (EACS, σ') were derived from the ratio of product to parent ion intensities and from absolute target gas pressure measurements. EACS are therefore absolute measurements of the reactivity of a mixture of ground and excited states. Provided monochromatic photons of selected energy were used, the relative population of these states is purely dependent on the energetics and the spectroscopy of the Ar^{2+} production. Conversely, if some higher order photons were emerging from the monochromator, they had the effect to perturb the population (e.g., by the production of excited states) and therefore led to a deviation from the rule mentioned above. For this reason, we used optimal higher order filtering while performing the measurements.

If the systematic uncertainty on the EACS is estimated to 25%, the random uncertainty is much lower, in the range of 5%. The

results shown here have been collected repeatedly, with a very good reproducibility.

Rare gases of high purity (Air Liquide, better than 99.995%) were used throughout all the experiments; D_2 and CH_4, from Matheson, had purity better than 99.9%. All gases were used without any further purification.

To obtain reliable data, the lifetime of the two excited states of Ar^{2+} should be much longer than the time necessary for dications to reach the reaction cell. The lifetime of the excited ^1S state has been the subject of extensive investigations [30]. Literature data agree around a value of 150 ms that is safely longer than our detection window. In the case of the ^1D state, its survival in the SWARM experiments [6] ensures that its lifetime is sufficiently long.

We systematically recorded reactant and product ion intensities as a function of the collision energy for each gas target, and we observed a decrease of reactivity, reaching a constant level at 0.5 eV collision energy in the center of mass (CM). We therefore chose to compare results for all targets at this collision energy of 0.5 eV CM. The cross-section data were transformed into rate constants by means of the relation:

$$k = \sigma\langle v\rangle$$

where k is a rate constant, σ is the cross-section, and $\langle v\rangle$ is the velocity of the center of mass.

2.1. The SU6 beamline at Super-ACO (low resolution)

The light source was the 16 permanent magnets, 1.33-m long, SU6 undulator inside the Super-ACO storage ring. When setting the minimum gap at 40.3 mm, the energy of the first harmonic was 32 eV. The light was monochromatised using a 1-m toroidal grating monochromator [31]. One "High flux–Low energy" grating was used to cover the photon energy range 43–52 eV. A toroidal mirror refocused the monochromatised light in the center of the ionization region of the apparatus. By using the first harmonic of the undulator, a typical flux of 10^{13} photons/s was available in the interaction region with a resolving power of $E/\Delta E = 400$. This beamline, known for its high flux, was chosen for the survey of Ar^{2+} reactivity with all the neutral targets hereby studied. The results showed a strong internal energy dependence of the reactivity and led to the request for further experimental time on the ELETTRA Synchrotron Gasphase Photoemission beamline, where higher photon energy resolution could be used, but for a limited time. We therefore restricted the high-resolution measurements to the two neutral targets showing the most different reactivity effects: He and D_2.

2.2. The gasphase photoemission beamline at ELETTRA (high resolution)

The layout of gas phase photoemission beamline at ELETTRA has been described elsewhere [25]. Briefly, vacuum ultraviolet and soft X-ray photons are emitted from an undulator source and dispersed by a spherical grating monochromator. In order to minimize the occurrence of higher order photons in the 43–52 eV range, we used a 400 l/mm grating, Al coated refocusing mirror and either one of two filters. The first filter (MgF_2) provided with very good removal of higher orders, but with an upper limit of transmission of 49.5 eV. It was used when recording the reactivity with He. The second filter (Al) was slightly less efficient in removing higher orders, but allowed collecting data in the whole energy range of interest, i.e., up to 52 eV. The optical set-up of the beamline, in our configuration, guaranteed a resolving power $E/\Delta E$ better than 1000. The calibration of the photon energy was checked during the measurements by means of the $^1P_0$ autoionizing Rydberg series of Ne located between 44 and 53 eV [32]. The photon beam intensity was continuously monitored using (i) the photoemission current from a gold grid (90% transmission) positioned along the beam path before the photoionization region and (ii) a photodiode (sodium salicylate scintillator) located at the exit of the photoionization region.

3. Results and discussion

In double photoionization, state selection of ions can be obtained by using multiple coincidence techniques but, at present, these techniques cannot be used to study ion–molecule reactions due to the very limited production rate of state-selected ions. A possible alternative consists in obtaining "state sensitive" information by scanning the wavelength of the ionizing radiation through the different Ar^{2+} states and studying the evolution of the various reaction channels. This is the method chosen in our case. The data are obviously different, so that we are able to go further in the analysis and derive some state-specific information.

In the following, we will first show the results obtained at high resolution to demonstrate the sensitivity of the method. We will then discuss the results obtained for the whole series of targets, at low photon energy resolution. Finally, we will present a method to obtain absolute state-selected cross-sections, and to derive from them an energy-dependent production branching ratio for the three dicationic states in the energy range that was investigated.

3.1. Spectroscopic information and effective absolute cross-sections

Fig. 1 shows the intensities of the parent dication Ar^{2+} and of the product ion Ar^+ recorded when scanning the photon energy

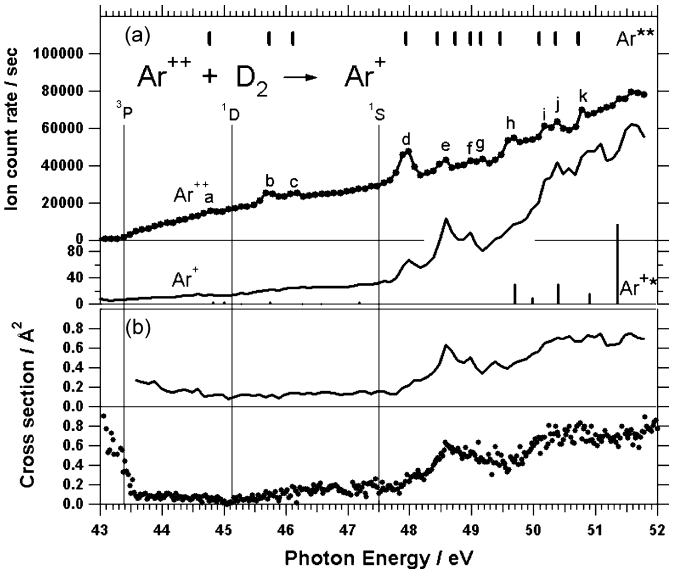

Fig. 1. (a) Photon energy dependence of the counting rates of Ar^{2+} parent dication and product Ar^+ monocation resulting from the charge transfer with D_2, measured on the gasphase beamline at ELETTRA Synchrotron. Thin vertical lines indicate the onsets of Ar^{2+} (^3P, ^1D, ^1S) states. Thick vertical lines of equal height (labelled Ar^{**}) represent the position of neutral states autoionizing into the dication continuum (from Ref. [34]), and thick vertical lines of variable length (labelled Ar^{+*}) represent the position and intensity (measured at 83 eV) of the singly charge ion excited states autoionizing to the dication continua from Ref. [35]. Features labelled from "a" to "k" are autoionizing structures identified in the dication yield. (b) Effective absolute cross-sections (EACS) σ' derived either from the upper signals (continuous line) or from the equivalent measurements performed on the SU6 beamline of the SuperACO Ring in LURE (dotted curve).

between 43 and 52 eV. The Ar^{2+} total yield (upper curve in Fig. 1a), exhibits a slow, almost linear, increase from the double photoionization threshold (43.39 eV), with no structures in the vicinity of the threshold of the first or second excited state (45.13 and 47.51 eV, respectively). Discrete resonances visible in the dication yield were observed earlier by Lablanquie et al. [33] at lower energy resolution. These structures, tagged from "a" to "k", can be ascribed either to neutral superexcited states Ar, or to excited states of the monocation Ar^{+*} (satellite channels), autoionizing into the dication continuum. Both processes were described for Ar^{2+} and we will show that it is possible to associate specific reactivity with the autoionizing structures.

Excited states of neutral Ar (Ar^{**}) are detected specifically in atomic photoabsorption. Madden et al. [34] have tabulated the energy of neutral states above the double photoionization threshold. They are described as two-electron excitation states of the generic type $3s3p^5nln'l'$. The authors do not propose a detailed assignment of the states and it is difficult to ascribe a configuration to the structures or to propose a preferential decay towards one of the three continua of Ar^{2+}. In any case, the position of most of the "Madden" resonances (reported in the upper part of Fig. 1a as thick vertical lines of equal height) is correlated with almost all the discrete features seen in the Ar^{2+} yield. Only one feature, labelled "h", appears in a region where no photoabsorption structure is reported.

Satellite states of Ar^{+*} located above the double ionization threshold have been investigated theoretically and experimentally by Combet-Farnoux et al. [35]. Photoelectron spectroscopy and coincidence methods were used to complement the work of Kikas et al. [36] who measured the binding energy of photoelectrons corresponding to the dication threshold. The position and intensity of satellite states are reported in the bottom part of Fig. 1a as thick vertical lines of height proportional to their intensities recorded at $h\nu = 83$ eV. If the most intense structure, corresponding to a configuration ($3s^23p^33d^2$) and located at 51.36 eV, is not clearly visible in the double ionization yield (probably because of a poor probability of population at its threshold), there is a structure at 49.69 eV which could be a good candidate to explain the feature labelled "h" in the dication yield, and would correspond to a configuration ($3s3p^5$), similar to the "Madden" series. A further argument to associate the "h" labelled structure to autoinizing monocation is its shape, which can be regarded more as a step function, instead of a peak.

High level theoretical methods such as configuration interaction (CI) were used to interpret the decay process of satellite Ar^{+*} channels. Combet-Farnoux et al. have shown that, above the threshold of the ^1D state, satellite states populated in the energy range investigated by us are decaying preferentially towards the ^1D continuum, few towards the ^3P continuum, and almost none towards the ^1S continuum. As a consequence, one can expect that the "h" labelled structure should correlate preferentially to a Ar^{2+} (^1D) continuum.

The lower curve in Fig. 1a represents the Ar^+ yield detected when Ar^{2+} reacts with D_2 in the reaction cell. It is worth mentioning the difference by three orders of magnitude between the parent and the product counting rates, indicative of very small reactivity cross-sections, as low as 0.2 Å^2, and peaking at 1 Å^2. From a qualitative comparison between parent and product signals, it is apparent that (i) Ar^+ yield shows a clear increase for energies higher than the ^1S threshold, (ii) structures labelled "d" and "h" are very much reduced in the Ar^+ ion yield, and (iii) faint structures in the dication yield, such as "e" and "f", lead to strong resonances in the product yield.

From these data, it is possible to extract the EACS by application of the procedure described in Section 2. The result is shown in Fig. 1b, as a continuous line for high-resolution measurements, or as dots for the low-resolution ones. The two results are in good quantitative agreement and confirm the abovementioned observations: (i) D_2 reacts poorly with dications in the ^3P or ^1D states,

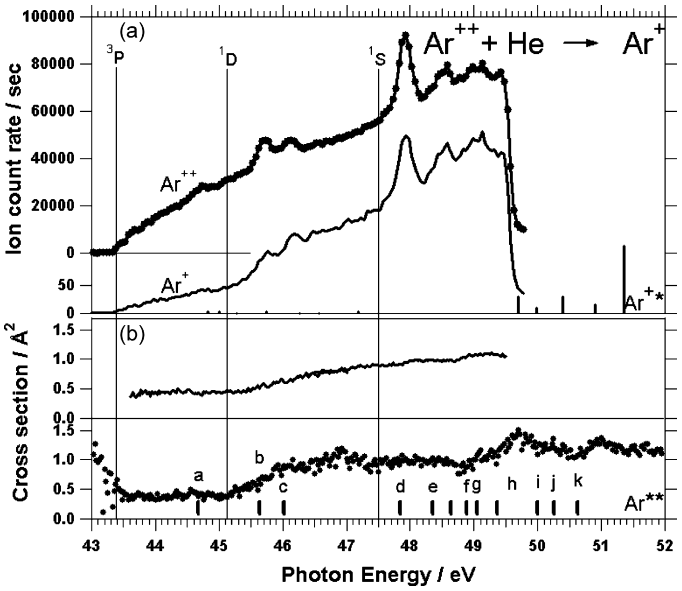

Fig. 2. (a) Photon energy dependence of the counting rates of Ar^{2+} parent dication and product Ar^+ monocation resulting from the charge transfer with He, measured on the gasphase beamline at ELETTRA Synchrotron, Trieste. Thin vertical lines indicate the onsets of Ar^{2+} (^3P, ^1D, and ^1S) states. Thick vertical lines of variable height (labelled as Ar^{+*}) represent the position and intensity (measured at 83 eV) of the singly charge ion excited states autoionizing to the dication continua from Ref. [35]. (b) EACS σ' derived either from the upper signals (continuous line) or from equivalent measurements performed on the SU6 beamline of the SuperACO Ring in LURE (dotted line). Thick vertical lines of equal size (labelled Ar^{**}) represent the position of neutral states autoionizing into the dication continuum (from Ref. [34]), while features labelled from "a" to "k"are the autoionizing structures identified in the dication yield of Fig. 1.

while showing a large increase in reactivity when ^1S state dications are present; (ii) some of the "Madden" resonances are enhanced in the reactivity ("e" and "f") and some are strongly depleted ("d" and "h"); (iii) the reduction of structure "h" is in perfect agreement with Combet-Farnoux et al. prediction, as it should correlate with ^1D continuum[35], which is poorly reactive.

EACS derived from high-resolution measurements (continuous line in Fig. 1b) exhibit a decrease in the energy region of the double ionization threshold, reaching a minimum close to the threshold of ^1D state production. This is not physically possible, as all dications in this energy range should be produced in their ground electronic state and therefore should exhibit a constant reactivity cross-section. The observed perturbation is due to the presence of a minor contribution of higher order photons from the gas phase monochromator, despite the use of the Al filter. Such a perturbation is also visible in the ion yield, as Ar^{2+} intensity below the double ionization threshold is not equal to zero. To avoid this problem when studying the reactivity with He, which from our low-resolution experiments was known to react preferentially in the ^3P and ^1D states, we inserted a MgF_2 filter when performing high-resolution measurements. Therefore, the ion yield measured below double ionization threshold is perfectly equal to zero (Fig. 2). The drawback is that the MgF_2 filter allows measurements only up to 49.4 eV. As a consequence, high-resolution data do not extend above the "g" structure of the Ar^{2+} yield and spectroscopy in that region has to be investigated only on the basis of low-resolution data (dotted curve in Fig. 2b).

Similarly to the D_2 case, in the studies of Ar^{2+} with He, the intensity ratio between parent and product ions is in the range of 1000, indicating a very small reactivity. There are however marked differences with the D_2 case: the Ar^+ ion yield mimics closely the Ar^{2+} one, except for a reduced reactivity in the region below the

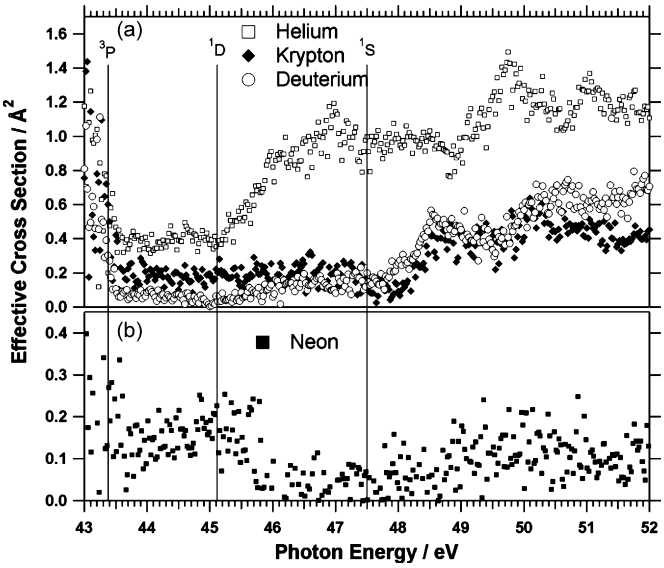

Fig. 3. Photon energy dependence of the EACS σ' for the charge transfer reaction of Ar^{2+} with (a) He, Kr and D_2 and (b) Ne. Data have been taken at a collision energy of 0.5 eV in the centre of mass frame. Thin vertical lines indicate the onsets of Ar^{2+} (^{3}P, ^{1}D, and ^{1}S) states.

^{1}D threshold (Fig. 2a). The EACS exhibits a flat intensity of 0.4 Å^2 in the low energy range where only the ^{3}P state can be populated, and increases smoothly from the ^{1}D threshold to reach a value of 0.8 Å^2 close to the ^{1}S threshold (Fig. 2b). All the resonant structures present in the Ar^{2+} yield vanish after treatment of high-resolution data. However, when looking at low-resolution data, "resonant" behaviour is clearly detectable in the vicinity of the "h" labelled structure. When enlarged (Fig. 3a), the EACS reveal also two other resonances, located at 46.9 and 51.0 eV, which do not correspond to any "Madden" resonance, and are therefore probably due to other monocation states autoionizing towards the ^{1}D continuum. In the case of reactions with He, we can draw the following conclusions: (i) He reacts poorly with Ar^{2+} (^{3}P), while showing a large increase of reactivity when ^{1}D dications are present; (ii) none of the "Madden" resonances are enhanced in the reactivity and (iii) the amplification of Ar^{**} autoionizing structures is in perfect agreement with Combet-Farnoux et al. prediction, as they should correlate with the reactive ^{1}D continuum.

From the results obtained on the two neutral targets we can conclude that D_2 reacts almost exclusively with the second excited state of Ar^{2+} (^{1}S), while He reacts preferentially with the first excited state (^{1}D). Moreover, some resonances appear in correlation with one or the other target. This is particularly evident for the feature labelled "h" in Figs. 1 and 2. The occurrence of resonances can be used to ascribe a decaying pathway of autoionizing states towards the specifically reacting continuum. Decaying pathway of the other structures is not known, but we propose that they are associated with excited states of neutral Ar [34]. For such features we can draw the following conclusions:

1. Structure labelled "a" is thermodynamically correlated to the ^{3}P ground state of the dication.
2. Structures labelled "b" and "c" may autoionize either to ^{3}P or ^{1}D continua and are not observed in the charge exchange cross-section with He and D_2. Therefore they do not decay specifically into any of the two energetically accessible Ar^{2+} states. One can expect a coupling to continua that should be close to statistical for these two structures.
3. Structure labelled "d" is visible, but depleted in the D_2 EACS and it is not observed in the He case. We therefore assume for this structure a behaviour showing no particular preference between the three continua, i.e., close to statistical behaviour between them.
4. Structures "e", "f" and "i", "j", "k" are enhanced in the EACS with D_2 and slightly depleted in the EACS with He, and therefore they most likely decay specifically into the ^{1}S continuum.

3.2. Effective absolute cross-section for all targets and comparison with previous results

In this part we will describe and compare with literature the state-specific reactivity measured at low resolution in the photon energy needed for single charge transfer process

$$Ar^{2+} + A \rightarrow Ar^{+} + A^{+}$$

where A = He, Ne, Kr, Xe, D_2, and CH_4

Let us note that literature values are expressed in rate constants and our measurements are cross-sections (EACS), but only the variations of these values with the Ar^{2+} state are discussed in this paragraph. See below for their conversion into rate constants.

3.2.1. He

Johnsen and Biondi [4] measured a thermal rate constant of 7×10^{-11} cm^3 s^{-1} for Ar^{2+} (^{3}P), 1.4×10^{-10} cm^3 s^{-1} for Ar^{2+} (^{1}D) and $<2 \times 10^{-14}$ cm^3 s^{-1} for Ar^{2+} (^{1}S) for this charge transfer process. State-selected rate constants for the Ar^{2+} (^{3}P) and Ar^{2+} (^{1}S) states in reaction with He have been obtained by SIFT [10,11] which are in good agreement with their investigation. Measured rate constants are 6.8×10^{-11} cm^3 s^{-1} and $<5 \times 10^{-13}$ cm^3 s^{-1} (i.e., below the detection limit of the instrument) for Ar^{2+} (^{3}P) and (^{1}S), respectively. Surprisingly, in these SIFT studies, Ar^{2+} (^{1}D) seems to be negligible in the primary Ar^{2+} beam, while its reactivity seems to be the largest among the three Ar^{2+} states. It is worth mentioning that Ar^{2+} (^{1}D) is efficiently produced by electron impact, as opposed to the previously mentioned SIFT findings. At low temperature (30 K) CRESU experiments [13] give a similar value of 6.2×10^{-11} cm^3 s^{-1} for the ^{3}P rate constant.

The dynamics of the charge transfer between Ar^{2+} (^{3}P, ^{1}D) and He has also been investigated in a crossed beam experiment by Friedrich and Herman [14,15]. By integrating angularly resolved data, it has been possible to determine a $\sigma(^1D)/\sigma(^3P)$ ratio of 3.12 at a center of mass collision energy of 0.53 eV, and deriving a rate constant of k (300 K) = 4.4×10^{-12} cm^3 s^{-1} for the charge transfer in good agreement with [4].

As shown in Fig. 3a, the value of EACS for He is nearly constant below the ^{1}D threshold at 45.12 eV. Above this energy, the cross-section rises up to 1 Å^2, showing three broad resonances (around 46.9, 49.7 and 51.0 eV). In the charge transfer spectrum, no clear evidence of the ^{1}S onset is detectable. This observation agrees with the results of all the swarm experiments, which measure a very small charge exchange rate constant for the ^{1}S state and a substantially larger value for the ^{1}D state when compared to the ground state.

3.2.2. D_2

The reaction $Ar^{2+} + H_2$ was studied by flow drift techniques by Lindinger et al. in the late 70s [9]. Under their experimental conditions, no reaction was observed. More recently, the rate of this reaction has been measured in drift experiments for Ar^{2+} (^{3}P) and (^{1}S) [10,12]. The rate constant for the ^{1}S state has been obtained by using the state-specific removal of Ar^{2+} (^{3}P, ^{1}D) in collision with He. Smith et al. [10] measured a rate constant of 1.6×10^{-12} cm^3 s^{-1}

for Ar^{2+} (^3P) and of 2.6×10^{-9} cm^3 s^{-1} for Ar^{2+} (^1S), while in [12] a rate of 1.3×10^{-9} cm^3 s^{-1} for the Ar^{2+} (^1S) reaction has been determined. These authors attribute such a discrepancy for the ^1S rate constant to the different experimental conditions. From a mechanistic point of view, the differences between the reactivity of the ^1S and ^3P states are explained by opening efficient reactive channels in the production of excited Ar^+ ions. The slow rate of the $Ar^{2+} + H_2$ reaction for ground state reactants has been confirmed at lower temperatures in CRESU experiments [13] (2.5×10^{-12} cm^3 s^{-1}).

From our experiment with D_2 (see Fig. 3a), the ^3P cross-section turns out to be close to the detection limit of our apparatus (~0.1 Å^2). This is in agreement with the previous investigations.

At photon energies above the ^1D onset, the EACS σ' shows a gentle rise, followed by a second increase after the ^1S threshold. Below this threshold, σ' is ~0.2 Å^2. Above ^1S, the evaluation of σ' is complicated by the presence of the "Madden" resonances described above. However, data taken at larger photon energy are consistent with an average value of 0.6 Å^2.

3.2.3. Kr

Drift tube results [4] indicate that this reaction proceeds efficiently only for Ar^{2+} (^1S). In this case a rate of 1.4×10^{-9} cm^3 s^{-1} was measured, which is close to the Langevin limit. This is in agreement with the SIFT experiment by Smith et al. [11] (1.0×10^{-9} cm^3 s^{-1}).

In our experiment (Fig. 3a) the EACS is very small, though not negligible, showing a constant value of 0.2 Å^2 for photon energies ranging from double ionization threshold to the Ar^{2+} (^1S) onset at 47.5 eV. Below the Ar^{2+} (^1D) onset, this value corresponds to the state-selected $\sigma(^3P)$ cross-section. At higher photon energies, no clear sign of the ^1D onset is observed and it is reasonable to suppose that the cross-section for this state is comparable to the previous one. A marked rise in the cross-section is noticeable in correspondence of the Ar^{2+} (^1S) and, above this limit, the EACS stabilizes around 0.4 Å^2.

3.2.4. Ne

Charge transfer process was investigated in swarm experiments [4,11], where it was found that reactivity was small. For the ^3P state of Ar^{2+}, the measured rate constants were 3.7×10^{-12} cm^3 s^{-1} [4] and 7×10^{-12} cm^3 s^{-1} [11], while for the ^1D state an upper limit of 3.7×10^{-12} cm^3 s^{-1} was given [4]. The least reactive state seems to be the ^1S, for which upper limits for the rate constant are 1×10^{-13} cm^3 s^{-1} [4] and 5×10^{-13} cm^3 s^{-1} [11].

For this system, our measurements can hardly be used to deduce quantitative data (see Fig. 3b). However, it is tentatively possible to detect a decrease in the EACS in correspondence of the Ar^{2+} (^1D) onset, following a trend already observed in He and D_2 (Fig. 3a), but in opposite direction. This evidence suggests that Ar^{2+} (^3P) is the most reactive state with Ne with an average cross-section of 0.15 Å^2.

3.2.5. Xe

For the single charge transfer channel, previous swarm experiments are in partial disagreement. Johnsen and Biondi [4] found that all the three Ar^{2+} states show similar values for the rate constants, with the ^1S slightly less reactive (^3P and ^1D 1.5×10^{-9} cm^3 s^{-1}, ^1S 1×10^{-9} cm^3 s^{-1}). Smith et al. [10,11] agreed in the ^1S value (1.5×10^{-9} cm^3 s^{-1}), but they have measured a smaller reactivity for the ^3P state (7.5×10^{-10} cm^3 s^{-1}).

Our measured EACS σ' (Fig. 4) shows a plateau at 8 Å^2 for the ^3P ground state followed by a slow decrease to 6 Å^2 between ^1D and ^1S thresholds. A further decline of EACS above the ^1S threshold support the idea that ^1D and ^1S states are slightly less reactive than the ^3P ground state, which confirms the results obtained in Ref. [4].

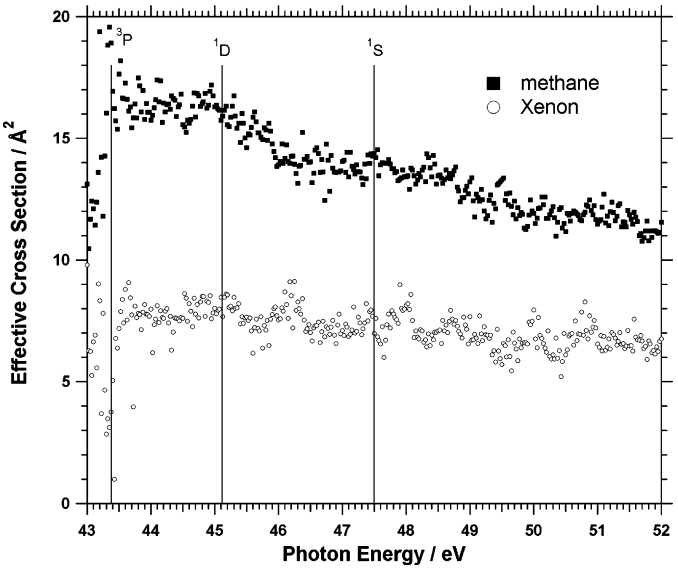

Fig. 4. Photon energy dependence of the EACS σ' for the charge transfer of Ar^{2+} with CH_4 and Xe. Data have been taken at a collision energy of 0.5 eV in the centre of mass frame. Thin vertical lines indicate the onsets of Ar^{2+} (^3P, ^1D, and ^1S) states.

3.2.6. CH_4

For this reaction, charge transfer and dissociative charge transfer was studied in a SIFT experiment [10] and reactive rate constant values very close to the Langevin limit (2×10^{-9} cm^3 s^{-1} for both ^3P and ^1S states) were measured. These authors report state selectivity in products formation, since ^3P leads mainly to non-dissociative charge transfer, while ^1S induces mainly dissociative charge exchange with formation of CH_2^+, CH^+ and H^+. In a different drift tube experiment [12], similar values for the rate constants were determined (2×10^{-9} cm^3 s^{-1} for ^3P and ~2.2×10^{-9} cm^3 s^{-1} for ^1S states).

Among the neutral target studied in the present work, methane had the largest cross-section. The EACS shows a plateau at 16.5 Å^2 at photon energies lower than the ^1D threshold. At higher energies, following a shape already described in He, D_2, and Ne cases, EACS decreases to ~14 Å^2 at the ^1S threshold (see Fig. 4). A further decrease was observed above the ^1S threshold. From this behaviour, a larger reactivity of the ground state compared to the first excited state can be deduced. However, a further contribution of the ^1S cannot be ruled out due to its very small relative abundance. Looking for state selectivity in the dissociative charge transfer channels, we investigated the photon energy dependence of the fragmentation channels leading to CH_3^+ and CH_2^+ but no sign of state sensitivity could be detected. Let us note that the charge exchange process between Ar^{2+} and CH_4 is mainly dissociative, no matter of the population of excited states in the Ar^{2+} beam. These results can be explained by considering the large exoergicity of the charge transfer reaction between Ar dications and methane.

3.3. From effective cross-sections to state selective cross-sections

We have shown that the collected data constitute a coherent set showing specific behaviour for each individual target. The general trend for each target is in agreement with the quantitative measurements of Johnsen and Biondi [4] and Smith et al. [10,11]. However, because of experimental limitations, the numerical values they provide for the reactivity of the ^1D state were either absent or affected by large uncertainties. Hereby we propose a method to extract state-selected cross-sections from the measured EACS as a function of the photon energy.

By measuring the Ar^{2+} total yield and the abundance of Ar^+ product ions, an "effective" absolute cross-section, σ', was obtained. This σ' corresponds to a state-selected cross-section only for the ground state Ar^{2+} (i.e., below the Ar^{2+} (^1D) threshold), otherwise it corresponds to the sum of the state-selected values, weighted by the branching ratio of the Ar^{2+} states produced at each photon energy. If we set I_a the counting rate of Ar^+ corresponding to the charge transfer process, I_0 the counting rate of the Ar^{2+} beam, $I_0(^3P)$, $I_0(^1D)$ and $I_0(^1S)$ the counting rates of Ar^{2+} ions in the ^3P, ^1D and ^1S states, respectively, we can write, in the thin target limit [29]

$$\sigma' = \frac{I_a}{nlI_0} \quad (1)$$

and

$$\sigma' = \sigma(^3P)\frac{I_0(^3P)}{I_0} + \sigma(^1D)\frac{I_0(^1D)}{I_0} + \sigma(^1S)\frac{I_0(^1S)}{I_0} \quad (2)$$

where n is the gas density, l is the scattering length and $\sigma(^3P)$, $\sigma(^1D)$, $\sigma(^1S)$ are the state-selected cross-sections. From the set of data shown in Figs. 3 and 4, we can extract state-selected cross-sections for the ^1D and ^1S by weighting the "effective" cross-section σ' with the relative abundance of each Ar^{2+} state.

As mentioned above, double ionization proceeds either directly or by autoionization of resonant states (either neutral or singly ionized). For this reason, the photoionization yield is due to resonant structures superimposed onto a linearly increasing continuum [33]. The branching ratio of the three Ar^{2+} states cannot be determined without knowing the specific decays of each autoionizing state. However, it has been shown [2] that the three states are populated according to their statistical weight at 48.4 eV photon energy and this rule seems to hold for Xe, Kr and Ar dicationic states, only few eV above thresholds. This means that below the ^1D threshold the population of the Ar^{2+} states are given by ^3P:^1D:^1S = 1:0:0; in the energy region above the ^1D and below the ^1S onsets the statistical weights are 0.64:0.36:0, while above the ^1S threshold the values are 0.60:0.33:0.07. As a consequence, if we extract from our EACS the "continuum" contribution once the plateau in the product yield is reached, we can obtain the state-selected cross-sections by using the statistical weights of the three ionic states. The final question is to define the energy at which we can safely assume to have the statistical branching behaviour. Obviously, below the ^1D threshold, the average EACS between double ionization and ^1D threshold can be used. For the energy region between the ^1D and ^1S onsets, the EACS was taken at 47.5 eV, i.e., away from the ^1D threshold, where clearly the population does not follow the statistical ratio, and away from the "b", "c" structures or from the monocation autoionizing structure identified in He EACS (see Figs. 1 and 2). Above the ^1S threshold the most appropriate energy value was determined in a similar way, i.e., away from threshold and resonances. We chose the excitation energy value of 51.5 eV.

Due to the indirect procedure and the empirical identification of photon energies at which statistical ratio between the states should be expected, the state-selected values that we propose for the excited states have an estimated uncertainty of 50% and 75% for ^1D and ^1S states, respectively. State-selected cross-sections extracted using this procedure are summarized in Table 1. Cross-section values have been transformed into rate constants, in order to ease the comparison with previous results compiled from the literature.

In He case, the ^1D reactivity (1.1×10^{-10} cm^3 s^{-1}) turns out to be at least a factor five higher than the ^3P (2.1×10^{-11} cm^3 s^{-1}) one, slightly smaller than the values obtained in swarm and crossed beam experiments. It is hard to derive a value for the ^1S state reactivity, as there is no evidence of a variation in the EACS above the ^1S threshold. But this is not conclusive due to the low statistical weight of the ^1S state near threshold. The ^1S abundance is highly

Table 1
State-selected cross-section and rate constant values for the charge transfer reaction of Ar^{2+} with neutral targets measured at a collision energy of 0.5 eV in the centre of mass frame

Neutral gas target	Ar^{2+} (^3P)				Ar^{2+} (^1D)			Ar^{2+} (^1S)		
	σ^a Å^2	k^a (cm^3 s^{-1})	k^b (cm^3 s^{-1})	k^c (cm^3 s^{-1})	σ^a (Å^2)	k^a (cm^3 s^{-1})	k^b (cm^3 s^{-1})	k^c (cm^3 s^{-1})	σ^a (Å^2)	k^a (cm^3 s^{-1})	k^b (cm^3 s^{-1})	k^c (cm^3 s^{-1})
He	0.4	2.1×10^{-11}	7×10^{-11}	6.8×10^{-11}	2.1	1.1×10^{-10}	1.4×10^{-10}	–	<1	<5.1×10^{-11}	<2×10^{-14}	<5×10^{-13}
Ne	0.15	4×10^{-12}	3.7×10^{-12}	3.7×10^{-12}	0	–	<3.7×10^{-12}	–	0.5 ± 0.5	$1.3 \pm 1.3 \times 10^{-11}$	<1×10^{-13}	<5×10^{-13}
Kr	0.18	3.4×10^{-12}	<2×10^{-13}	<5×10^{-13}	0.18	3.4×10^{-12}	<2×10^{-13}	–	5 ± 3	$9.4 \pm 6 \times 10^{-11}$	1.4×10^{-9}	1×10^{-9}
Xe	8	1.4×10^{-10}	1.5×10^{-9}	7.5×10^{-10}	7.4	1.3×10^{-10}	1.5×10^{-9}	–	< 6.6	<1.2×10^{-10}	1×10^{-9}	1.5×10^{-9}
D_2	0.06	3.1×10^{-12}	–	1.6×10^{-12}	0.40	2.1×10^{-11}	–	–	8 ± 2	$4.1 \pm 1 \times 10^{-10}$	–	2.6×10^{-9}
CH_4	16.5	4.8×10^{-10}	–	2×10^{-9}	11.8	3.4×10^{-10}	–	–	<5	<1.5×10^{-10}	–	2×10^{-9}

The values are extracted from a treatment, assuming that statistical population of states exists at 47.5 and 51.5 eV, photon energies.
[a] This work.
[b] Rate constants measured at room temperature using SWARM [4,5].
[c] Rate constants measured at room temperature using SIFT [10,11].

enhanced in the photon energy range around 48.6 eV (Fig. 3a), as discussed in D_2 and Kr cases. Thus, a significant reactivity of the ^1S state, would imply an increase in effective cross-section, whereas experimental data show a dip in the corresponding photon energy region. We can therefore confirm the result of Johnsen and Biondi that state-selected ^1S reactivity is negligible with respect to the reactivity of the ^1D.

The reactivity with neon is always small, but the extracted rate constant value for ^3P (4×10^{-12} cm^3 s^{-1}) is in excellent agreement with previous results. The ^1D state reactivity is probably extremely small confirming the Johnsen and Biondi upper limit [4]. In addition, the evaluated rate constant for the ^1S state suffers from the same limitation as for the He experiment, hence the value extracted from our analysis has a high degree of uncertainty.

In the case of Kr, $\sigma(^3P)$ and $\sigma(^1D)$ have similar values of 0.2 Å^2, while the ^1S excited state is the most reactive with $\sigma(^1S)$ equal to 5 ± 3 Å^2. From the σ' value below the ^1D threshold we obtain a state-selected rate constant for the ^3P and ^1D states of 3.4×10^{-12} cm^3 s^{-1}, close to the detection limit of our apparatus. From the σ' value at high photon energy (in the range 51–52 eV) we estimate a value of $9.4 \pm 6 \times 10^{-11}$ cm^3 s^{-1} for the ^1S state reactivity rate constant, i.e., 30 times larger than the two other states, but one order of magnitude lower than the previously reported values.

In Xe case, from the averaged values of σ' in the energy region below the threshold for formation of Ar^{2+} (^1D), a value of 1.4×10^{-10} can be deduced for the state-selected ^3P rate constant. From the averaged σ' at 47.5 eV, a value of $1.3 \pm 6 \times 10^{-10}$ is obtained for ^1D rate constant. For the ^1S state, only an upper limit of the rate constant can be given, due to the small relative abundance of the ^1S state in the Ar^{2+} beam. All our numerical values for this target are one order of magnitude lower than the previously reported ones.

In D_2 case, from the σ' value below the ^1D threshold we obtain the state-selected rate constant for the ^3P state of 3.1×10^{-12} cm^3 s^{-1}, close to the detection limit of our apparatus, and in fairly good agreement with the result of Smith et al. [10]. From the measured σ' value in the energy region below the onset of the ^1S threshold we get a value of 2.1×10^{-11} cm^3 s^{-1} for the ^1D state reactivity. From the σ' value at high photon energy (in the range 51–52 eV) we estimate a value of $4.1 \pm 1 \times 10^{-10}$ cm^3 s^{-1} for the ^1S state reactivity rate constant.

Finally, in CH_4 case, a larger reactivity of the ground state can be deduced and a value of 4.8×10^{-10} cm^3 s^{-1} and 3.4×10^{-10} cm^3 s^{-1} can be obtained for ^3P and ^1D rate constant, respectively. As for the Xe and He case, only an upper limit of the $\sigma(^1S)$ cross-section can be given due to the small relative abundance of the ^1S state in the Ar^{2+} beam. The values are once again one order of magnitude lower than previously reported ones.

3.4. Energy-dependent production yield of the three states of Ar^{2+} dication

Looking at Figs. 3 and 4, it appears that the measured EACS result from the linear combination of three patterns. The first pattern would be a flat signal associated with the energy range where only ^3P state is produced, the second one would be a component starting at the ^1D threshold and reaching a plateau at about 46 eV, and the third one would start at the ^1S threshold and reach a plateau at about 48.5eV. We performed a principal component analysis (PCA) [37] on the full set of EACS. It confirmed the clear presence of the three features described above.

From Eq. (2), if a target shows a strong specificity of reactivity with one dicationic state, the formula can be simplified, and the variations of EACS σ' are directly linked to the relative intensity of the specific state in the total mixture of states ($\sigma' = k \times I_0(x)/I_0$). Using the EACS of He, we extracted the $I_0(^1D)/I_0$. Kr and D_2 data were used to derive the $I_0(^1S)/I_0$. $I_0(^3P)/I_0$ was simply recovered by normalising the previous signals at 47.5eV for the ratio $^3P/^1D$ and at 51.5 eV for the ratio $^3P/^1D/^1S$.

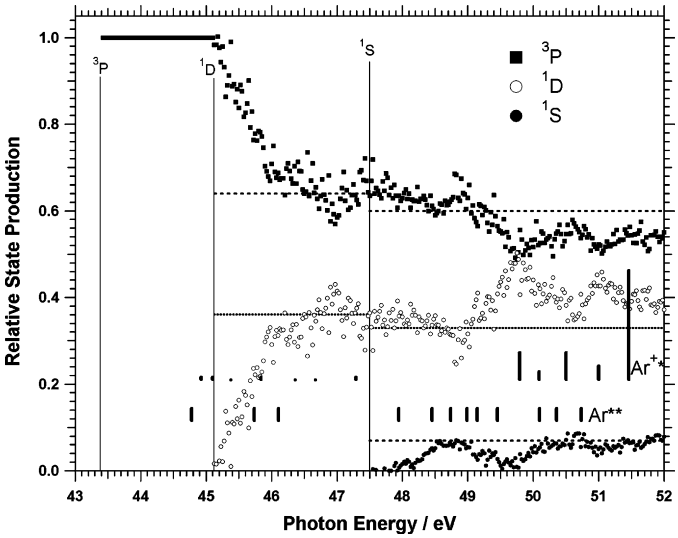

Fig. 5. Photon energy dependence of the ^3P, ^1S and ^1D states of the Ar^{2+} dication. Dotted lines represent the relative levels that should be observed in case of statistical population of the states. Thin vertical lines indicate the onsets of Ar^{2+} (^3P, ^1D, and ^1S) states. Thick vertical lines of equal size represent the position of neutral states autoionizing into the dication continuum (from Ref. [34]), and thick vertical lines of variable height represent the position and intensity (measured at 83 eV) of the singly charge ion excited states autoionizing in the dication continua from Ref. [35].

The result of this treatment is displayed in Fig. 5, where the photon energy-dependent production branching ratio of the dication three electronic states is plotted.

In the energy range below ^1D threshold, the relative amount of ^3P is one by definition. In the energy range between the ^1D and ^1S thresholds, ^3P and ^1D states coexist. Fig. 5 reveals that the relative intensity of the first excited state starts to increase linearly directly from threshold to reach the statistical ratio (0.66/0.33) approximately 1 eV above the ^1D threshold. There is a minor deviation from the statistical ratio at the photon energy of ~46.9 eV. We associate it with the presence of an Ar^{+*} autoionizing state. With the exception of this feature, the ratio stays flat until the ^1S threshold. In the energy range where the three states can coexist, the behaviour of the ^1S state is markedly different as it stays at a very low level for the first 0.5 eV above threshold, and then exhibits a resonant behaviour in correspondence of the structures identified at high-resolution in Fig. 1 and associated to autoionizing neutral states Ar**. This resonant character is confirmed by the fact that the relative production of the ^1S state is greatly reduced in an energy range around 49.5 eV where no resonance is present. The relative production of the ^1S state increases again in correspondence with new autoionizing features, to reach the statistical value at roughly 51 eV, i.e., 4.5 eV above the threshold. In that energy range, the relative production of the ^1D state has a constant value with two resonances corresponding to two autoionizing monocation states Ar^{+*}. Due to the small relative population of the ^1S state, the Ar^{2+} (^3P) state is basically acting as a reservoir losing intensity when ^1D is increasing. Let us note that the assumption of statistical population of the states postulated at 51.5 eV is questioned by the deviation of ^3P and ^1D states from the statistical ratio, but we reproduce the statistical ratio determined by Eland et al. at 48.4 eV [2].

4. Conclusions

Charge exchange cross-sections of Ar^{2+} dications with several neutral target (He, Ne, Kr, Xe, D_2, and CH_4) were measured and strong state-specific effects were observed when different Ar^{2+} electronic states (^3P, ^1D and ^1S) are produced by direct double photoionization of Ar using tunable synchrotron radiation in the range from 43 to 52 eV. From charge transfer yields measured for different targets, state-selected cross-sections were deduced assuming a statistical production of the three Ar^{2+} electronic states upon direct ionization. Using the above information, an energy-dependent production yield for the three dicationic states in the investigated energy range can be extracted. This finding is of interest from a spectroscopic point of view since it allows the identification of preferential decay pathways of resonant states (Ar^{**} and Ar^{+*}) present above the double ionization threshold.

Acknowledgments

It is the authors' pleasure to dedicate this work to Zdenek Herman, at the occasion of his 75th birthday. Zdenek has published many milestone papers in the field of gas phase dication reactivity. His sharp understanding of processes associated to his ability to work out picturing conclusion from results will stay as a very good memory. It is our pleasure to have him as co-author, collaborator, and friend.

The authors wish to thank Jana Roithova (IOCB AVCR, Prague Czech Republic) for her supportive help in the data acquisition sessions held in Orsay. The ELETTRA and SuperACO staff are kindly acknowledged for operating the synchrotron rings and beamlines. In particular, we would like to thank Damiano Avi, Michele Alagia, Robert Richter, Bertrand Pilette and Gérard Bellec for their technical assistance during the installation and running of the experiment at ELETTRA.

P.F., D.A. D.B. and P.T. acknowledge funding by the Italian Government PRIN through Contract Nos. 2003035479 and 2005033911. Partial support of this research by the Grant Agency of the Academy of Sciences of the Czech Republic (IAAA400400702) is gratefully acknowledged. O.D. and C.A. acknowledge funding from the IA-SFS European Network Contract.

References

[1] Y. Ralchenko, F.-C. Jou, D.E. Kelleher, A.E. Kramida, A. Musgrove, J. Reader, W.L. Wiese, K. Olsen, NIST Atomic Spectra Database (version 3.1.2) (online) available http://www.physics.nist.gov/asd3 2007, National Institute of Standards and Technology, Gaithersburg, MD.
[2] J.H.D. Eland, O. Vieuxmaire, T. Kinugawa, P. Lablanquie, R.I. Hall, F. Penent, Phys. Rev. Lett. 90 (2003) 053003-1.
[3] A. Huetz, P. Selles, D. Waymel, J. Mazeau, J. Phys. B 24 (1991) 1917.
[4] R. Johnsen, M. Biondi, Phys. Rev. A 20 (1979) 989.
[5] R. Johnsen, M. Biondi, Phys. Rev. A 18 (1979) 996.
[6] R. Johnsen, M. Biondi, Phys. Rev. A 18 (1978) 989.
[7] L.D. Landau, Z. Phys. 1 (1932) 88.
[8] C. Zener, Proc. R. Soc. A 137 (1932) 696.
[9] W. Lindinger, E. Alge, H. Störi, M. Pahl, R.N. Varney, J. Chem. Phys. 67 (1977) 3495.
[10] D. Smith, D. Grief, N.G. Adams, Int. J. Mass. Spectrom. Ion Phys. 30 (1979) 271.
[11] D. Smith, N.G. Adams, E. Alge, H. Villinger, W. Lindinger, J. Phys. B: Atom. Mol. Phys. 13 (1980) 2787.
[12] H. Störi, E. Alge, H. Villinger, F. Egger, W. Lindinger, Int. J. Mass. Spectrom. Ion Phys. 30 (1979) 263.
[13] G. Dupeyrat, J.B. Marquette, B.R. Rowe, C. Rebrion, Int. J. Mass. Spectrom. Ion. Proc. 103 (1991) 149.
[14] B. Friedrich, Z. Herman, Chem. Phys. Lett. 107 (1984) 375.
[15] B. Friedrich, S. Pick, L. Hladek, Z. Herman, E.E. Nikitin, A.I. Reznikov, S.Y. Umanskii, J. Chem. Phys. 84 (1986) 807.
[16] D. Schröder, J. Loos, H. Schwarz, R. Thissen, J. Roithova, Z. Herman, Int. J. Mass Spectrom. 230 (2003) 113.
[17] J. Roithová, D. Schröder, J. Loos, H. Schwarz, H. Jankowiak, R. Berger, R. Thissen, O. Dutuit, J. Chem. Phys. 122 (2005) 094306.
[18] O. Hadjar, D. Ascenzi, D. Bassi, P. Franceschi, M. Sabidò, P. Tosi, Chem. Phys. Lett. 400 (2004) 476.
[19] P. Tosi, R. Correale, W. Lu, S. Falcinelli, D. Bassi, Phys. Rev. Lett. 82 (1999) 450.
[20] J. Roithova, R. Thissen, J. Zabka, P. Franceschi, O. Dutuit, Z. Herman, Int. J. Mass Spectrom. 228 (2003) 487.
[21] J. Roithova, J. Zabka, J. Hrusak, R. Thissen, Z. Herman, J. Phys. Chem. A 107 (2003) 7347.
[22] J. Roithova, J. Zabka, R. Thissen, Z. Herman, Phys. Chem. Chem. Phys. 5 (2003) 2988.
[23] J. Jasik, J. Roithová, J. Zabka, Z. Herman, R. Thissen, D. Schroeder, H. Schwarz, J. Phys. Chem. A 108 (45) (2006) 9931.
[24] P. Franceschi, R. Thissen, J. Žabka, J. Roithová, Z. Herman, O. Dutuit, Int. J. Mass Spectrom. 228 (2003) 507.
[25] P. Franceschi, D. Ascenzi, P. Tosi, R. Thissen, J. Zabka, J. Roithovà, C.L. Ricketts, M. De Simone, M. Coreno, J. Chem. Phys. 126 (2007) 13431.
[26] O. Witasse, O. Dutuit, R. Thissen, J. Zabka, C. Alcaraz, J. Lilensten, P.-L. Blelly, S.W. Bougher, S. Engel, L.H. Andersen, K. Seiersen, Geophys. Res. Lett., doi:10.1029/2002GL014781.
[27] C. Simon, J. Lilensten, O. Dutuit, R. Thissen, C. Alcaraz, O. Witasse, H. Soldi-Lose, Ann. Geophys. 23 (2005) 781.
[28] O. Dutuit, C. Alcaraz, D. Gerlich, P.M. Guyon, J.W. Hepburn, C. Métayer-Zeitoun, J.B. Ozenne, M. Schweizer, T. Weng, Chem. Phys. 209 (1996) 177.
[29] K.M. Ervin, P.B. Armentrout, J. Chem. Phys. 83 (1985) 166.
[30] E. Träbert, G. Gwinner, Phys. Rev. A 65 (2001) 014501.
[31] J.M. Bizau, E. Bouisset, C. Blancard, J.P. Champeaux, A. Compant la Fontaine, C. Couillaud, D. Cubaynes, D. Hitz, C. Vinsot, F.J. Wuilleumier, Nucl. Instrum. Methods B 205 (2003) 290.
[32] K. Schulz, M. Domke, R. Puttner, A. Gutierrez, G. Kindl, G. Miecznik, G.H. Greene, Phys. Rev. A 54 (1996) 677.
[33] P. Lablanquie, J.H.D. Eland, I. Nenner, P. Morin, J. Delwiche, M.J. Hubin-Franskin, Phys. Rev. Lett. 58 (1987) 992.
[34] R.P. Madden, D.L. Ederer, K. Cordling, Phys. Rev. 177 (1969) 136.
[35] F. Combet-Farnoux, P. Lablanquie, J. Mazeau, A. Huetz, J. Phys. B: Atom. Mol. Phys. 33 (2000) 1597.
[36] A. Kikas, S.J. Osborne, A. Ausmees, S. Svensson, O.P. Sarainen, S.J. Aksela, Electron Spectrosc. Relat. Phenom. 77 (1996) 241.
[37] E.R. Malinowski, Factor Analysis in Chemistry, 3rd ed., John Wiley, 2002.